arXiv:hep-ex/0102051 28 Feb 2001

SOFT HADRONIC INTERACTIONS

PETER SCHLEPER
DESY, Notkestr. 85, 22607 Hamburg, Germany
E-mail: Peter.Schleper@desy.de

Recent developments in soft hadronic interactions are reviewed. Emphasis it put on measurements of the proton structure at low x, photon structure, diffraction and exclusive processes such as vector-meson production and their interpretation in approaches to QCD dynamics like BFKL or CCFM.

1 Introduction

Quantum Chromodynamics is the generally accepted field theoretical prescription of strong interactions and is successfully applied to processes where a hard scale is present, given by either a highly virtual particle, a large transverse momentum or a large mass of the exchanged particles[1]. In such processes the strong coupling constant is small enough to allow for perturbative calculations and QCD is predictive. In soft processes, where such a hard scale is not present, α_s becomes large and perturbative techniques are not applicable. This prohibits predictions of such fundamental quantities as the size and mass of the proton, the total cross-section for hadron-hadron scattering or cross-sections for elastic scattering of hadrons. All these questions are closely connected to confinement and still belong to the least well understood properties of strong interactions.

In the past many phenomenological models have been developed to describe soft interactions. More recently, driven by new data obtained in the transition region between soft and hard processes from the HERA, LEP and Tevatron experiments, the theoretical interpretation within perturbative QCD (pQCD) has made considerable progress. This is also the focus of this review[a], and hardly any reference is given to phenomenological prescriptions of soft physics.

[a] Plenary Talk, ICHEP 2000, Osaka.

Deep Inelastic Scattering

To introduce the concepts it is useful to start with the example of deep inelastic scattering (DIS) of a lepton on a proton (Fig. 1). Here

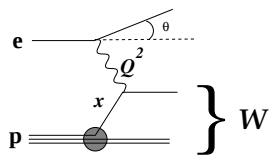

Figure 1. Feynman diagram for deep inelastic scattering.

Q^2 denotes the virtuality of the exchanged photon γ^*, the Bjorken scaling variable x corresponds in lowest order to the momentum fraction of the struck quark in the proton and W is the total centre of mass energy in the γ^*-proton system. For $Q^2 \gg \Lambda^2_{QCD}$ the high γ^* virtuality provides the hard scale and the structure of the proton is resolved into partons, i.e. the cross-section is proportional to the structure function $F_2(x, Q^2)$ which measures the quark momentum distribution in the proton. Fig. 2 shows the data on F_2 as obtained by fixed target experiments and at HERA[2], which now cover a Q^2 range from several 10^4 GeV^2 down to $\simeq \Lambda^2_{QCD}$, and include momentum fractions x as low as 10^{-6}. The data nicely demonstrate the point-like nature of quarks in the region of approximate scaling at $x \approx 0.1$, modified by negative scaling violations at higher x which are attributed to the quark splitting $q \to qg$ and, at low x, by positive scaling violation due to the prevailing gluon splitting $g \to gg$, $q\bar{q}$.

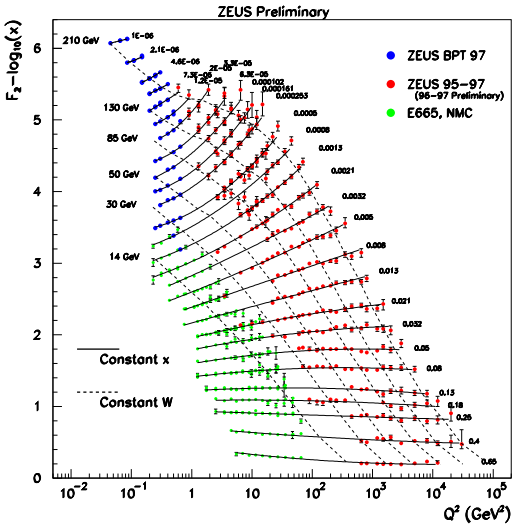

Figure 2. Proton structure function F_2 as a function of Q^2 with lines of constant x and W from [2].

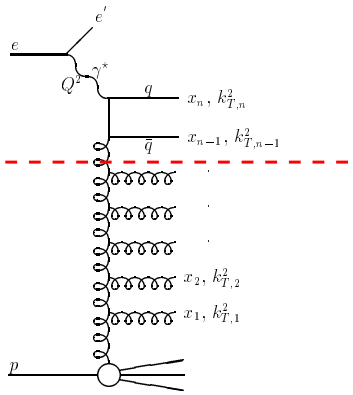

Figure 3. The parton ladder in a hard scattering process. The dashed line denotes the factorisation into a hard matrix element and the parton density.

The sharp increase of F_2 with decreasing x at Q^2 values of a few GeV^2, the main result of the first HERA data [5], is of great importance as this slope is directly related to the gluon density in the proton. The proton at low x is thus a system of very high gluon density and thereby a unique environment for the understanding of QCD dynamics. Since $W^2 = Q^2(1-x)/x$, the extrapolation towards low x at fixed Q^2 corresponds to the high energy (W) limit of QCD, which is interesting in itself but also has impact for e.g. cosmic ray experiments, heavy ion collisions and Higgs production at the LHC via $gg \to H$ [9].

QCD Dynamics at Low x

To better understand the present excitement about low x dynamics it is worth recalling the assumption of *factorisation* of hadronic cross-sections into a matrix element of the hard process (which is calculable in pQCD) and parton distribution functions which represent all other soft parts of the diagrams (Fig. 3). In the standard Altarelli-Parisi (DGLAP[11]) evolution the phase-space for parton emission is approximated by summing those contributions where the transverse momenta $k^2_{T,i}$ along the ladder strictly increase from the proton to the hard scattering, and therefore is applicable only at larger Q^2. To this approximation the process factorises into calculable coefficient functions and supposedly universal parton distribution functions which obey the DGLAP evolution equations.

It is apparent that other momentum configurations will contribute both at low Q^2 and at low x. At low Q^2 (i.e. Q^2 not much larger than Λ^2_{QCD}) at any point along the ladder $k^2_{T,i}$ might exceed Q^2 which destroys the required strong k_T ordering. Even at higher Q^2 but low x_n, the large possible differences between the longitudinal momenta x_i imply sufficient phase-space also for large transverse momenta k_T somewhere along the ladder, again affecting strong k_T ordering. The transition region from high to low Q^2 and the low x limit thereby elucidate other approaches to pQCD and hence to QCD dynamics.

If the strong k_T ordering criterion is relaxed the approximations become more complex. For the BFKL[13] and CCFM[14] evolution equations ordering in x or in the emission angle of partons along the ladder is assumed, respectively. The resulting "unintegrated" parton densities depend directly on the trans-

verse momenta k_T as shown in Tab. 1. The

Table 1. QCD evolution equations based on different ordering schemes, the dependence of the parton density functions (pdf), the terms summed and the kinematic range of application.

	DGLAP	BFKL	CCFM
order	k_T	x	angle
pdf	$f(x,Q^2)$	$f(x,k_T^2)$	$f(x,k_T^2,Q^2)$
$\sum$	$\ln Q^2$	$\ln 1/x$	$\ln Q^2$ + $\ln 1/x$
valid	high Q^2 high x	$k_T^2 \approx Q^2$ low x	low x

BFKL approximation is expected to be valid only at low x, since it does not contain the DGLAP terms. It is not known yet how low Q^2 or x have to be to yield sizeable BFKL type contributions. The CCFM equation would in principle enable a smooth extrapolation between the DGLAP and the BFKL regime as it contains both parts. Up to now it is only applicable at low x since the quark splitting terms are not known yet.

Vector-Meson Production

An intriguing view of the interplay between soft and hard physics is derived from *elastic photoproduction* ($Q^2 \approx 0$) of vector-mesons at HERA[6], $\gamma p \to Vp$. For vector-mesons consisting of light quarks (ρ, ω) the energy dependence of the cross-section $\sigma_{\gamma p \to Vp}$ is very weak and similar to the total photon-proton cross-section (Fig. 4). For the J/Ψ, however, the energy dependence is significantly stronger, indicating that the charm quark mass provides a hard scale. The size of the cross-section is hence not of geometrical nature but can be associated with the partonic content of the proton. In this case the process is assumed to be dominated by the exchange of a pair of gluons which together form a colour singlet to yield an elastically scattered proton (Fig. 5). The increase of the cross-section towards large W reflects the increase

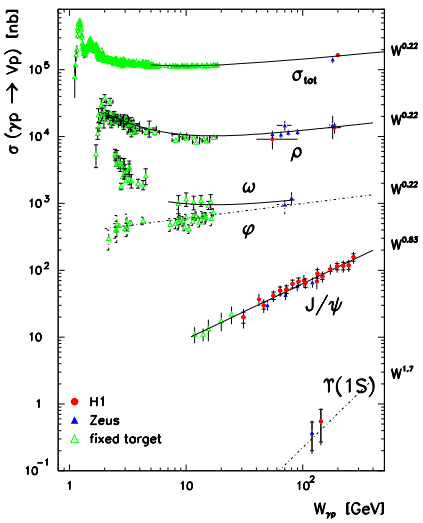

Figure 4. Energy dependence of the total photon-proton cross-section σ_{tot} in comparison to the cross-section for elastic photoproduction of vector-mesons from HERA [6].

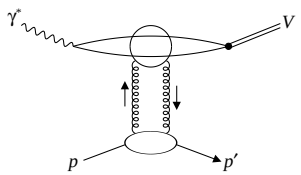

Figure 5. Feynman diagram for the production of vector-mesons V on an elastically scattered proton via 2-gluon exchange.

of the gluon density (squared) towards low x.

It is evident that in the extreme high energy limit this behaviour must change since the J/Ψ contribution should never exceed the total cross-section. New dynamics must therefore dampen the J/Ψ cross-section in the high W (low x) limit.

In QCD calculations[15] the cross-section is explained as a three step process: the splitting of the photon into a $q\bar{q}$ dipole, the interaction of this dipole with the gluon pair and finally the formation of the vector-meson. At low Q^2 and low x the three steps take place on very different time scales suggesting that the cross-section factorises into the probabil-

ities for each of the individual steps.

This factorisation allows the same dipole cross-section to be applied also in other processes at low x such as inclusive DIS, jet production or diffraction[7,8].

2 The Proton at Low x

The proton structure at low x is of interest not only as a new domain in QCD, where fundamental insight into the dynamics within and beyond the perturbative regime is still to be gained. It is also of relevance for the program at the Tevatron and the LHC[9]. For the small Higgs mass expected due to the indirect and direct measurements at LEP [10] the dominant production process $gg \to H$ (with $M_H = x_1\, x_2\, s_{\rm LHC}$) at LHC energies implies gluon momenta x_i in the range $1 > x > 10^{-4}$, or $0.1 > x > 10^{-3}$ if the angular acceptance for the Higgs decay products is restricted to rapidities $|y| < 2$. Sensitive tests of the Higgs sector therefore crucially depend on the gluon density at low x and the reliability of the theoretical extrapolation from low to high Q^2 [9]. At and below $x = 10^{-3}$ the only process giving access to the gluon density in the proton is DIS at HERA.

HERA Data and the Gluon Density

Both HERA collaborations H1 and ZEUS have released new preliminary data[2,3] on their structure function measurements in the low x and low Q^2 region. The H1 data[3] shown in Fig. 6 have now in a large range a statistical precision of $\approx$ 1% and systematic errors of about 3% due to new instrumentation such as silicon tracking and high granularity calorimetry. This represents important progress in comparison to existing published data, and the precision is probably close to the final results attainable by the experiments in parts of the phase-space. To determine simultaneously α_s and the gluon density at low x, the H1 collaboration has subjected this data to an elab-

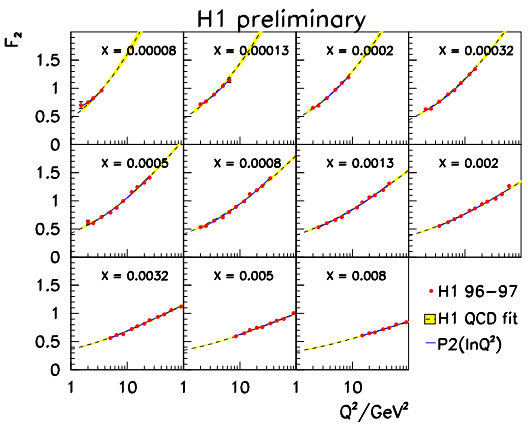

Figure 6. The proton structure function F_2 at low x as a function of Q^2 from H1 [3,4].

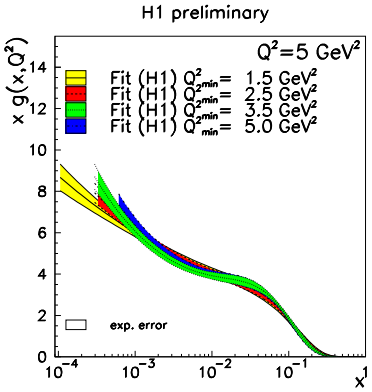

Figure 7. The gluon density obtained by H1 [4] in a DGLAP fit for different minimal Q^2_{min} values of the input data.

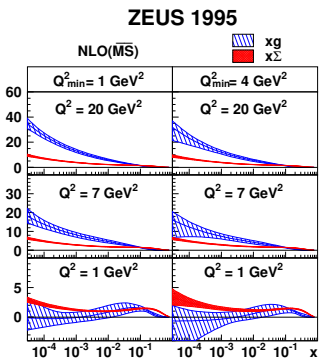

Figure 8. The gluon density (xg) and quark singlet density ($x\Sigma$) at medium and low Q^2 from ZEUS[17].

orate NLO QCD fit taking into account all experimental and theoretical systematic uncertainties [4]. A value of $\alpha_s(M_Z^2) = 0.1150 \pm 0.0017(stat.) \pm 0.0011(model) \pm 0.005(scale)$ was obtained. The largest uncertainty, arising from the choice of the renormalisation and factorisation scale, is expected to be reduced significantly once NNLO calculations become available[12]. The gluon density is constrained to $\approx 3\%$ for $10^{-3} < x < 0.1$ at $Q^2 = 20$ GeV^2. The fit describes the data well[4] down to $Q^2 \gtrsim 1$ GeV^2, but below $Q^2 = 5$ GeV^2 the resulting gluon distribution becomes sensitive to the inclusion of data at smaller and smaller Q^2 (Fig. 7). This more precise result confirms the previous finding [16,17] that the role of the gluon and quark density change when going to low values of Q^2 (Fig. 8). At low x the gluon density dominates the proton structure for $Q^2 \gg 1$ GeV^2, but tends to vanish at $Q^2 \approx 1$ GeV^2. The parton density functions appear to be flexible enough for the NLO DGLAP fit to accommodate the inclusive F_2 data down to $Q^2 \approx 1$ GeV^2, and also describe the longitudinal structure function F_L [4]. Nevertheless this "valence"-like behaviour of the gluon density is likely to signal the limit of applicability of the perturbative series in DGLAP. It might imply that higher twist effects or new dynamics such as described by the BFKL equation become sizeable. More exclusive data would be highly welcome in this low x region [19].

The Low x and Low Q^2 Limit

Since the CMS energy at HERA is limited to $\sqrt{s} = 320$ GeV kinematics imply that values of $x < 10^{-4}$ are accessible only at *very* low $Q^2 < xs$. Both H1 and ZEUS have equipped the region close to the beam axis with small calorimeters and silicon trackers which are able to measure down to $x \approx 10^{-6}$ for $Q^2 \gtrsim \Lambda^2_{QCD}$ (Fig. 9). New data from ZEUS [2] complement previous measurements

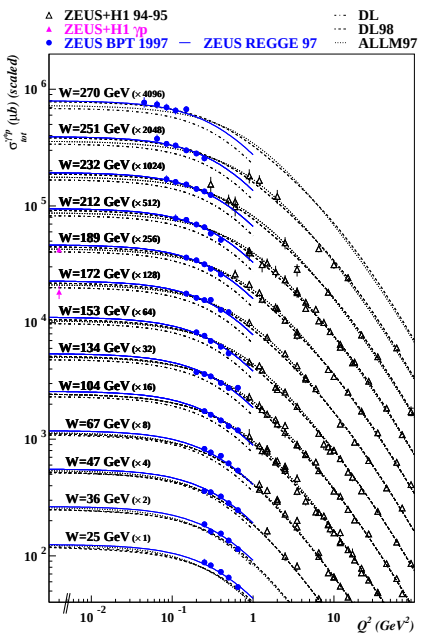

Figure 9. The total cross-section for γ^*-proton scattering as a function of Q^2 for constant values of W from HERA[2]. Also shown are two measurements for $Q^2 \approx 0$, from [20].

on $\sigma_{\gamma^* p} \sim F_2/Q^2$ and allow interpolation between the steep fall of the cross-section at high Q^2 and the photoproduction region at $Q^2 \approx 0$, where the cross-section must become independent of Q^2 because of conservation of the electromagnetic current. In other terms, the photon in the limit $Q^2 \to 0$ fluctuates into a hadronic object of similar size as the proton, such that the "dipole"-proton cross-section becomes independent of the exact value of Q^2 [b]. The precise form of $\sigma_{\gamma^* p}$ has been subject to considerable discussions[18,8] about the onset of a possible recombination (or saturation) of the gluon density in this region of low x and high gluon density. Fig. 10 shows slopes $\left(\partial F_2/\partial \log Q^2\right)_{\text{fixed } x}$, which to first approximation are directly proportional

[b] Unfortunately this constant behaviour of the dipole cross-section in the limit $Q^2 \to 0$ is sometimes referred to as "saturation", which is not the same as saturation of parton densities in the proton at higher Q^2 due to recombination effects.

to the gluon density. For all Q^2, and especially $Q^2 \gtrsim 1$ GeV^2 where the picture of a proton resolved into partons is applicable, this slope rises linearly towards low x. No deviation from this behaviour is visible in the energy range accessible at HERA[c]. In summary the inclusive HERA data do not provide evidence for saturation effects of parton densities for Q^2 above a few GeV^2. At smaller Q^2 where the photon itself develops hadronic structure, low x effects are difficult (if not impossible) to disentangle from low Q^2 effects.

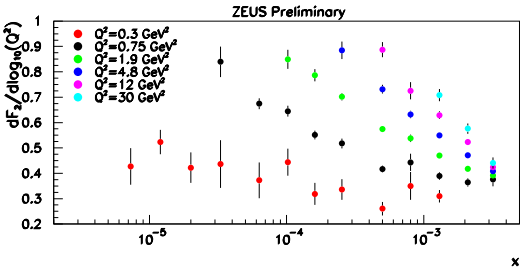

Figure 10. The derivative $(\partial F_2/\partial \log Q^2)_{\text{fixed } x}$, as a function of x in bins of Q^2 based on data from fixed target experiments and from ZEUS [2].

3 The Photon as a Hadronic Object

A quasi-real photon of very small virtuality ≈ 0 not only couples to other particles directly as a gauge boson or as a $q\bar{q}$ dipole of small transverse size (the point-like component which is calculable in pQCD) but can also fluctuate into a hadron-like object of large transverse size. The hadronic structure of the photon can be measured in the processes[21,22]:

- $e^+e^- \to e^+e^-\gamma^*\gamma \to e^+e^-X$ where the virtual γ^* resolves the structure of the real γ (Fig. 11). This process is mainly sensitive to the quark densities in the γ. The gluon density in the photon is only accessible indirectly via the scale dependence which requires very precise data.

- $ep \to e\gamma p \to e + jets + X$ at HERA where jets with large transverse energy are required to resolve the γ structure. Since coloured partons of the proton enter the hard interaction, this process is sensitive directly to both the quark and gluon density of the γ.

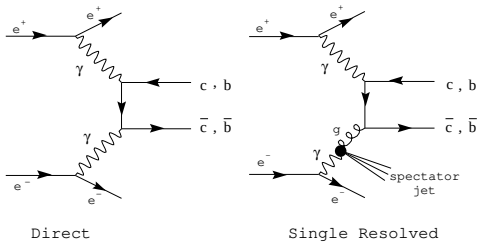

Figure 11. Example for a direct (left) and single resolved (right) $\gamma\gamma \to$ hadrons process in e^+e^- interactions, shown here for heavy quarks.

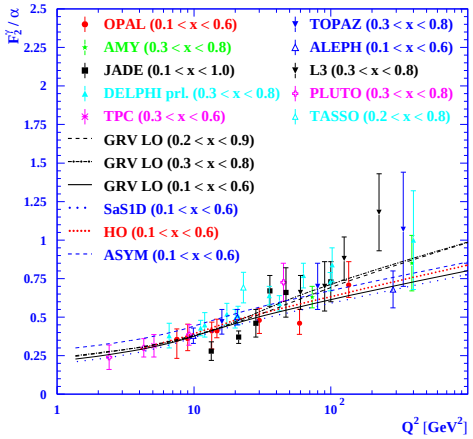

Figure 12. The structure function $F_2^\gamma(x, Q^2)$ for real photons from e^+e^- scattering[21,23] as a function of the scale Q^2 at which the γ is probed. Note that Q^2 here denotes the virtuality of the γ^* which probes the quasi-real photon of virtuality ≈ 0.

The LEP experiments have recently made substantial progress in the understanding of

[c] Note that the data shown here is identical to that in a much debated figure where the same slope is shown in bins of W. Due to the kinematic relation $W^2 = Q^2(1-x)/x$ this figure however shows a peak at Q^2 values of a few GeV^2, which should not be interpreted as saturation of parton densities.

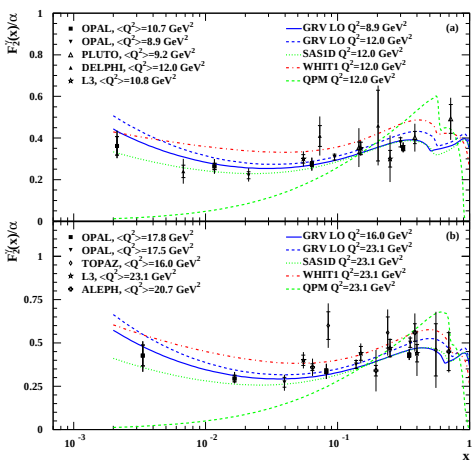

Figure 13. The photon structure function F_2^γ from e^+e^- scattering[24] at low and high Q^2 as a function of x. The QPM line which vanishes at low x corresponds to the quark-parton model approximation to the point-like component.

both the simulation of the hadronic final state and the detector response close to the beam direction. Improved unfolding methods have led to much more precise measurements and also to better consistency between the experiments. The LEP II data now are superior to all previous data from e.g. the PETRA experiments, and in addition give access to the photon structure at much larger scales and at lower x. Fig. 12 and 13 show that the photon structure function F_2^γ is now known with a precision of $\approx 10\%$. The basic expectations for the behaviour of F_2^γ are:

- F_2^γ is dominated at high x by the point-like part.
- F_2^γ rises with Q^2, in contrast to the proton case, for all x_γ due to the point-like contribution.
- At low x the hadron-like component is expected to dominate and the photon becomes similar to the proton, i.e. F_2^γ rises strongly towards low x and the photon is dominated by gluons.

The first two points are clearly borne out in the data shown in Fig. 12 and 13 when comparing with the expectation for the point-like component. The hadron-like component is seen at low x as the data clearly exceed the point-like part, although the expected rise of F_2^γ at very low x is not significant in the accessible x range. Note that existing parameterisations of the γ structure like GRV(LO) describe the data well for $Q^2 > 5$ GeV^2. Heavy flavour production data from LEP[25] are shown in Fig. 14. For charm production

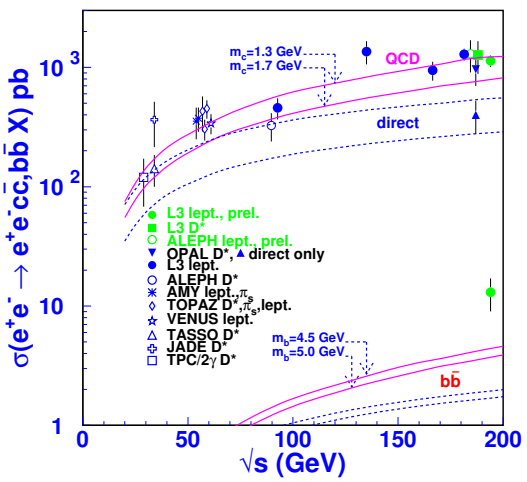

Figure 14. The charm and bottom cross-section from $\gamma^*\gamma$ scattering at LEP[25].

the data agree well with QCD expectations based on the same parameterisations. A first measurement of the charm structure function $F_{2,c}^\gamma$ has been obtained by OPAL[26] (Fig. 15). The bottom cross-section as measured by L3

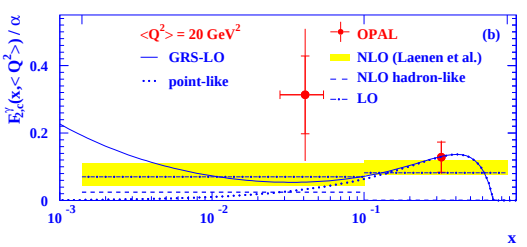

Figure 15. The charm structure function $F_{2,c}^\gamma$ from OPAL[26].

[25] is larger than expected (Fig. 14), a very interesting observation as the same trend is observed also by the Tevatron experiments

and in photoproduction at HERA. These observations require the theoretical description of heavy flavour production processes in hadronic collisions to be reconsidered.

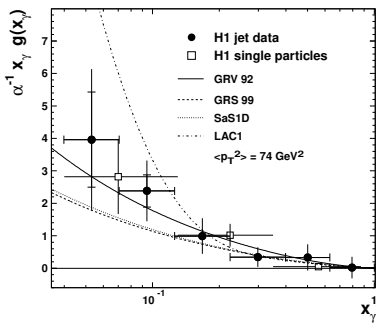

Figure 16. The gluon density in the photon as measured by H1[28].

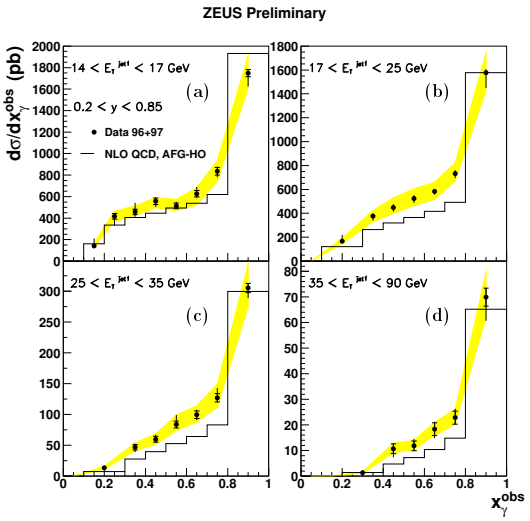

Figure 17. Jet cross-section in γp interactions from ZEUS[29].

Further access especially to the gluon component in the γ is obtained from jet production at HERA. In an analysis tailored towards the low x region, the H1 experiment has used data at relatively low transverse jet energies $E_T > 6$ GeV which was corrected for the substantial effects of secondary interactions between the photon remnant and the proton remnant in resolved photon processes. Subtracting the direct and quark induced parts based on expectation from e^+e^- data, the gluon distribution in the γ is extracted (Fig. 16). Albeit only in LO this is the only experimental evidence for a rise of parton densities in the photon at low x.

A complementary analysis by ZEUS[29] uses jets at much larger E_T, which kinematically excludes the low x region. Here the experimental and theoretical uncertainties are smaller however. In the range $0.3 < x < 0.8$ the ZEUS data are consistent with the NLO calculations for $14 < E_T < 17$ GeV, but exceed the calculations for larger E_T (Fig. 17). A similar effect was seen in a first jet measurement in e^+e^- scattering by OPAL [30].

Note that this poses a question on the overall consistency of the photon structure data. The LEP F_2^γ data, which are sensitive mainly to quarks up to scales of $\lesssim 800$ GeV^2, as well as the H1 data on gluons and quarks at low x, agree with e.g the GRV parameterisation. The ZEUS jet data, also sensitive to quarks and gluons but at high x and high E_T where the point-like component should dominate and little freedom due to the hadron-like component is expected, indicate an increased scale dependence of the parton densities, an effect which is difficult to understand.

The improved precision of the data in an extended x and Q^2 range calls for a new effort in the understanding of the photon structure in NLO QCD. Whether parton densities can be derived which consistently describe all data sets within errors remains to be seen.

4 QCD Dynamics at Low x

In spite of the fact that the inclusive proton structure function F_2 is compatible with the DGLAP evolution equations even at the lowest accessible x values (for $Q^2 \gtrsim 1$ GeV^2), it is still expected that $\ln 1/x$ terms must become sizeable in comparison with the $\ln Q^2/\Lambda^2_{QCD}$ terms if only x is small enough.

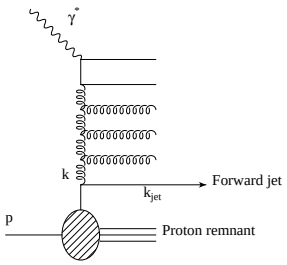

Figure 18. Parton ladder with a hard "forward" jet close to the proton remnant direction.

Considerable effort is therefore expended at HERA, as well as at LEP and Tevatron, into the investigation of more exclusive processes [32,31]. The advocated[33] test case at HERA is the production of "forward jets" (Fig. 18), i.e. a jet close in rapidity to the proton. In such events, when the jet transverse energy E_T is comparable to the photon virtuality at the other end of the parton ladder, k_T ordered radiation should be suppressed and parton emission might dominate which is not ordered in k_T.

Fig. 19 shows the cross-section for forward jets as a function of E_T^2/Q^2 from ZEUS[34]. None of the DGLAP based calculations are able to explain the data everywhere. Calculations based on structure functions for *virtual photons* have been available since several years, where for the case $E_T^2 \gg Q^2$ the γ^* is assumed to be resolved by the E_T of the jets. Starting from the highest E_T somewhere along the ladder, two parton cascades are then evolved towards the photon and the proton. As this corresponds to $non-k_T$ ordering, it may be viewed as an approximation to new QCD dynamics such as those predicted by the BFKL or CCFM equations. Calculations based on resolved virtual photons are indeed able to explain the data both in the DGLAP regime at $E_T \ll Q^2$ or $E_T \gg Q^2$ and in the BFKL regime at $E_T \approx Q^2$. Apart from these data only weak evidence for BFKL type dynamics exists up to now [31,32].

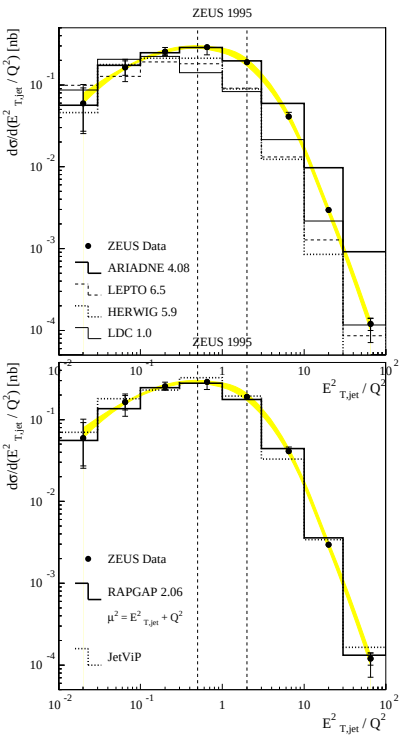

Figure 19. Cross-section for forward jet production from ZEUS[34] in comparison to calculations based on: upper figure: DGLAP (LEPTO and HERWIG) and colour-dipole model (ARIADNE); lower figure: resolved virtual photons in LO (RAPGAP) and NLO (Jetvip).

Similar to the forward jet case, deep inelastic production of charm is a two-scale process and thus a test-case for effects beyond k_T ordering. Fig. 20 shows the charm production cross-section in comparison to DGLAP and CCFM based calculations. Note that the calculation makes use of unintegrated parton densities $f(x, k_T^2, Q^2)$ which are obtained from a fit to the H1 F_2 data[35]. While deviations from the data are present in both approaches, the CCFM calculation does better especially in the forward direction at large pseudorapidities η close to the proton. This test of CCFM dynamics looks promising also in details of the final state.

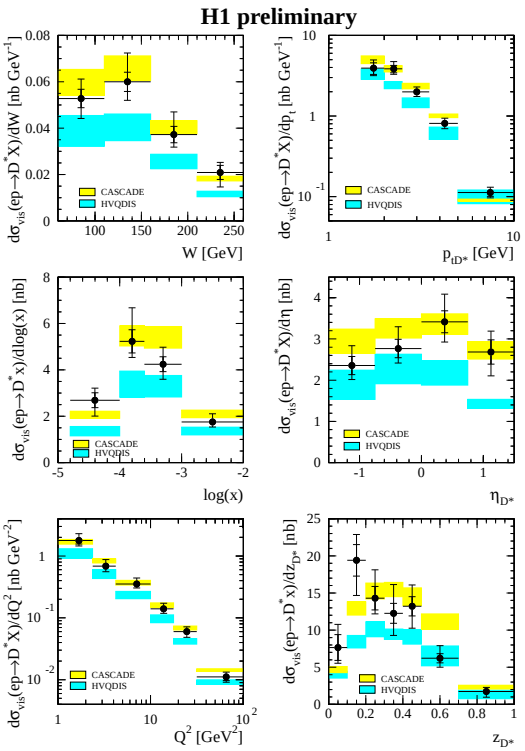

Figure 20. Cross-section for D^* mesons from H1[36] as a function of W, x and Q^2 together with the transverse momentum P_{T,D^*}, pseudorapidity η_{D^*} and momentum fraction z of the D^*. HVQDIS and CASCADE are NLO DGLAP and CCFM based calculations, respectively.

5 Diffraction

Processes in which a proton is scattered elastically are a challenge to pQCD calculations as they must proceed via a colour singlet exchange, in contrast to the standard approximation of single quark or gluon exchange. These processes are of fundamental interest as, in the end, they address the nature of colour confinement in QCD[38].

From *soft* hadronic processes it is known that beyond the expected exchange of photons and mesons, an additional component must be present, which can not be associated to any known particle[d]. This colour singlet exchange has generally been assumed to be dominated by gluons, however its precise nature remained unclear.

The interest in diffraction was renewed when *hard* diffractive processes were observed in $p\bar{p}$ collisions[39] and ep collisions [40], in which the partonic structure of the colour singlet exchange can be resolved.

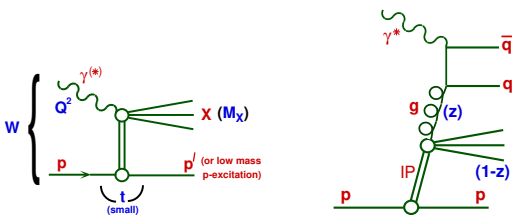

Figure 21. Feynman diagrams for diffractive scattering in $\gamma^* p$ collisions at HERA; inclusive scattering (left) and di-jet production (right).

Hard Diffraction at HERA

Fig. 21 shows the diagram for deep inelastic, inclusive diffractive scattering. The corresponding cross-section depends on four kinematic quantities: x, Q^2, the momentum transfer squared t at the proton vertex and the momentum fraction $x_{I\!P}$ of the colour singlet relative to the proton.

Important theoretical progress was recently achieved by the proof of QCD hard scattering factorisation [41] for diffractive ep scattering[e], which states that the cross-section factorises into hard partonic cross-sections and universal diffractive parton distributions $f_i^D(x, Q^2, x_{I\!P}, t)$. The latter should evolve (at fixed $x_{I\!P}$ and t) according to the DGLAP evolution equations. This proof puts diffraction on a solid basis for a treatment in pQCD and experimental verification is highly desirable.

For inclusive diffractive scattering the HERA experiments usually integrate over t

[d] In the framework of Regge theory[37] this exchange was labelled "pomeron" ($I\!P$).

[e] Note that factorisation is expected to break down in $p\bar{p}$ collisions due to secondary interactions between the two protons.

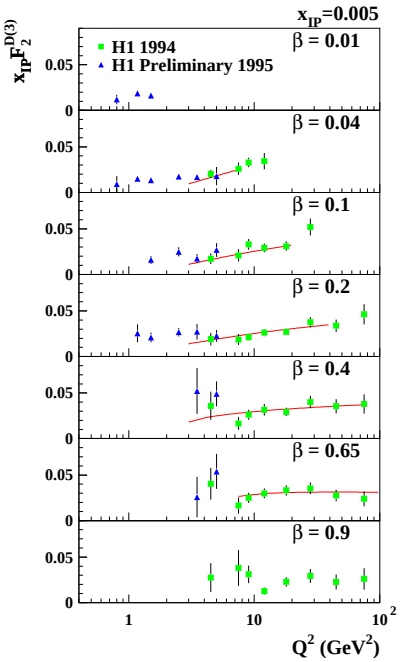

Figure 22. The diffractive structure function $F_2^{D(3)}$ from H1[42,43].

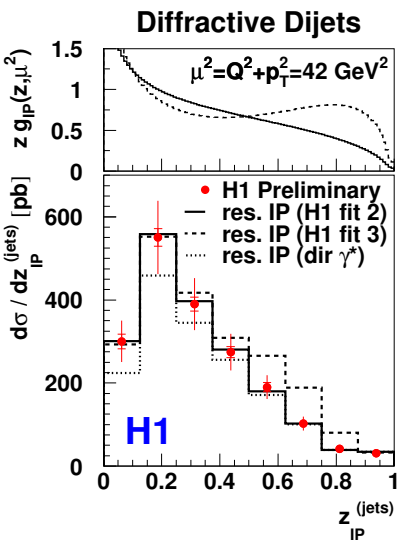

Figure 23. Diffractive di-jet cross-section from H1[44] (bottom) in comparison to predictions based on gluon densities (top) extracted by two QCD fits to the H1 $F_2^{D(3)}$ data. Here $z_{I\!P}$ corresponds to β for inclusive diffractive scattering.

and present their result as a structure function $F_2^{D(3)}(\beta, Q^2, x_{I\!P})$ (Fig. 22), where $\beta = x/x_{I\!P}$ corresponds to the momentum fraction of the struck parton in the colour singlet exchange. The data[42] show positive scaling violations up to large β, indicating the dominance of gluons in the diffractive exchange.

Assuming in addition Regge factorisation[37], $F_2^{D(3)}$ can be written as a flux factor for the colour singlet $f_{(x_{I\!P},t)}$ times a structure function for the exchange $F_2^D(\beta, Q^2)$. QCD fits of the scaling violation in $F_2^D(\beta, Q^2)$ yielded gluon densities[42] as shown in Fig. 23 (top).

A direct measure of the gluon distribution can be obtained from di-jet production in diffraction (Fig. 21). The new data from H1[44] (Fig. 23) are compatible with both Regge and QCD factorisation and nicely confirm the previous $F_2^{D(3)}$ analysis which assumed Regge factorisation. A new, QCD based calculation of this diffractive cross-

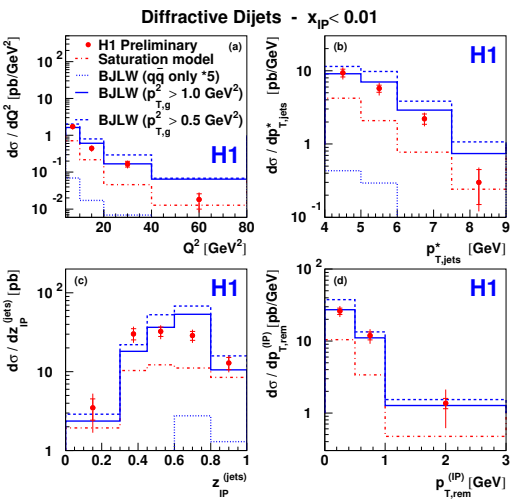

Figure 24. Diffractive di-jet cross-section from H1[44] in comparison to calculations (BJLW) based on the exchange of 2 gluons which interact dominantly with a $q\bar{q}g$ fluctuation of the γ.

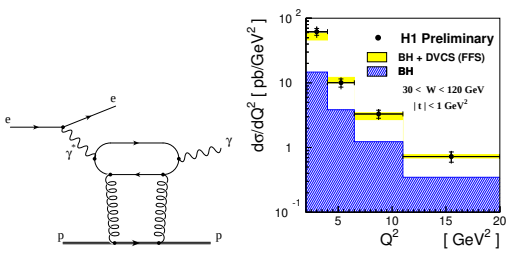

Figure 25. Feynman diagram and cross-section for Deeply Virtual Compton Scattering (DVCS) from H1[46]. The process interferes with the Bethe-Heitler (BH) process $ep \to e\gamma p$ (where the γ is emitted from the electron line) for which the contribution is shown separately.

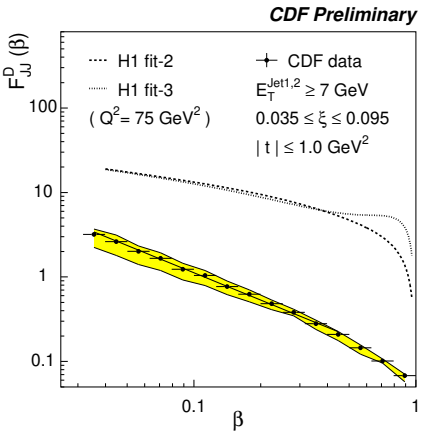

Figure 26. The diffractive structure function extracted from jet data by CDF[48] in comparison to an expectation based on the H1 diffractive parton densities.

section, which assumes dominant exchange of two gluons interacting with the $q\bar{q}(g)$ system emitted by the virtual photon (c.f. Fig. 21), leads to a reasonable description of the data at small $x_{I\!P}$ (Fig. 24). Again unintegrated gluon densities are employed here. Similar calculations have also become available for the diffractive production of vector-mesons (Fig. 4) and for Deeply Virtual Compton Scattering $\gamma^* p \to \gamma p$ (DVCS) (Fig. 25). It is remarkable that perturbative calculations are now able, with only a few free parameters, to describe a number of hard diffractive processes in ep scattering. It would be of high interest to complement these data with measurements at high t where the colour-singlet itself might be calculable in pQCD.

Hard Diffraction at the Tevatron

Both D0 and CDF have investigated processes where jets with large E_T are employed to study the partonic structure of the diffractive exchange. The most striking observation is that the overall rate of diffractive processes is much smaller (by factors 5 to 20 [47]) in comparison to the findings at HERA, where they contribute as much as 10% to the DIS cross-section.

Fig. 26 shows the effective structure function from jets F_{jj}^D from CDF for events where the elastically scattered proton was tagged at very small scattering angles. The data are far below a calculation which is based on the H1 parton densities extracted from $F_2^{D(3)}$ (Fig. 23). QCD factorisation obviously is badly broken for diffractive $p\bar{p}$ collisions. The same conclusion is obtained using only Tevatron data from the ratios of double- to single and single to non-diffractive cross-sections, which are significantly different (Fig. 27). It is noted that the QCD factorisation proof for ep scattering does not apply to $p\bar{p}$ collisions. The large factorisation

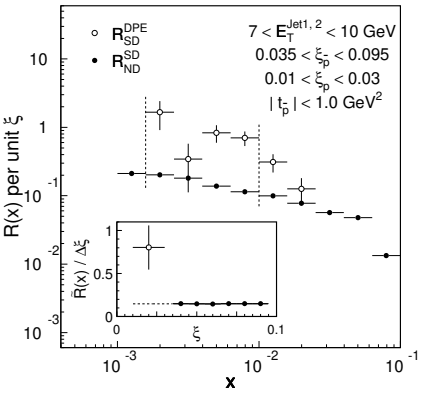

Figure 27. Ratios of double to single diffractive cross-sections R_{DPE}^{SD} and single to non-diffractive cross-sections R_{SD}^{ND} from CDF[49].

breaking observed when extrapolating from HERA results to Tevatron processes reflects that a point-like virtual photon (or a $q\bar{q}$ fluctuation of small transverse size) is able to pass through the proton without destroying it, whereas two large proton remnants will destroy each other in most cases. While this prohibits at present an interpretation of the $p\bar{p}$ data in terms of universal diffractive parton densities, the mechanism of factorisation breaking is in itself of interest and a challenge for the understanding of diffraction in hadron-hadron collisions[50].

6 Conclusion

Among the most active fields of QCD are the regions where perturbative approaches are difficult, namely at large distances close to the confinement limit, at high energies or low x, in regions of large parton densities and where multi-parton exchange becomes crucial. The entire field is driven by the availability of very precise data which are needed for detailed tests of QCD.

At low $x \gtrsim 10^{-3}$ the structure function data from HERA constrain the gluon density with a precision of better than 3% at high Q^2, which paves the way for significant tests of the Higgs sector at the Tevatron/LHC. While conventional DGLAP evolution describes the inclusive data down to $Q^2 \gtrsim 1$ GeV, more exclusive measurements of the hadronic final state indicate the need for calculations beyond strong k_T ordering. Evidence for BFKL effects from HERA, LEP or Tevatron are still weak, in spite of the fact that theoretical uncertainties seem to be better controlled[31]. The first CCFM calculations based on parton densities unintegrated in k_T look promising when compared with HERA data on charm production.

The LEP and HERA experiments have provided data on the photon structure with much improved precision. As existing photon parton densities seem not to be sufficient to describe all measurements a new effort in the understanding of the photon structure in NLO QCD is required.

In diffraction the comparison between hard inclusive and exclusive processes at HERA has led to a consistent picture of the structure of diffractive colour singlet exchange which is dominated by gluons. A challenge here is the application of the HERA results to hadron collisions, where QCD factorisation in diffraction is shown to be broken.

Acknowledgements

It is a pleasure to thank the organizers, Y.Yamazaki and the technical staff in Osaka for their help, K. Borras, J. Dainton, E. Elsen, B. Foster, M. Klein, P. Newman and R. Nisius for useful comments to the manuscript and many others for valuable discussions.

References

1. R. Nania, these proceedings.
2. A. Pellegrino, these proceedings; also [3].
3. M. Klein, proceedings Lepton-Photon 1999, SLAC.
4. F. Zomer, these proceedings.
5. H1 Coll., *Nucl.Phys.* **B407** (1993) 515; ZEUS Coll., *Phys.Lett.* **B316** (1993) 412.
6. B. Mellado, these proceedings.
7. B.L.Ioffe, *Phys.Lett.* **30B** (1969) 123.
8. K.Golec-Biernat, M.Wüsthoff, *Phys.Rev.* **D59** (1999) 014017; M.McDermott, hep-ph/9912547, and references therein.
9. S. Catani et. al., hep-ph/0005025, hep-ph/0005114.
10. A.Gurtu, these proceedings; P. Igo-Kemenes, these proceedings, and talk at the LEPC Nov.3rd, 2000.
11. Y. Dokshitzer, *Sov. Phys. JETP* **46** (1977) 641; V. Gribov, L. Lipatov, *Sov. J. Nucl. Phys.* **15** (1972) 438 and

675; G. Altarelli, G. Parisi, *Nucl.Phys.* **B126** (1977) 298.
12. W.L. van Neerven, A. Vogt, hep-ph/0006154; A.D. Martin et. al., hep-ph/0007099.
13. E.Kuraev, L.Lipatov, V.Fadin, *Sov. Phys. JETP* **45** (1977) 199; Y. Balittski, L. Lipatov, *Sov. J. Nucl. Phys* **28** (1978) 822; L. Lipatov, *Sov. Phys. JETP* **63** (1986) 904.
14. M.Ciafaloni, *Nucl.Phys.* **B296** (1988) 49; S. Catani, F. Fiorani, G. Marchesini, *Phys.Lett.* **B234** (1990) 339, *Nucl.Phys.* **B336** (1990) 18; G. Marchesini, *Nucl.Phys.* **B445** (1995) 45.
15. M. Ryskin et. al., *Z. Phys.* **C76** (1997) 231; L. Frankfurt et. al., *Phys.Rev.* **D57** (1998) 512.
16. H1 Coll., contr. paper ICHEP 1997, Jerusalem.
17. ZEUS Coll., *Eur.Phys.J.* **C7** (1999) 609.
18. B. Foster, hep-ex/0008069, and references therein.
19. U. Maor, these proceedings.
20. S. Levonian, these proceedings.
21. R. Nisius, *Phys.Rept.* **332** (2000) 165.
22. M. Erdmann, Springer Tracts in Modern Physics 138 (1996), DESY-96-090.
23. R. Nisius, private communication.
24. OPAL Coll., , CERN-EP-2000-82.
25. A. Böhrer, these proceedings.
26. OPAL Coll., *Eur.Phys.J.* **C16** (2000) 579.
27. H1 Coll., *Phys.Lett.* **B467** (1999) 156.
28. H1 Coll., *Phys.Lett.* **B483** (2000) 36.
29. ZEUS Coll., *Eur.Phys.J.* **C11** (1999) 35.
30. Th. Wengler, these proceedings.
31. L.H. Orr, these proceedings.
32. H1 Coll., *Phys.Lett.* **B462** (1999) 440; D0 Coll., B.Pope, these proceedings; L3 Coll., M.Wadhwa, these proceedings.
33. A. Mueller, *Nucl.Phys. (Proc.Suppl.)* **18C** (1991) 125, *J.Phys.* **G17** (1991) 1443; J. Kwiecinski, *Eur.Phys.J.* **C9** (1999) 611.
34. ZEUS Coll., *Phys.Lett.* **B474** (2000) 223.
35. H. Jung, DIS workshop 1999, hep-ph/9905554; S.Baranow, H.Jung, N. Zotov, hep-ph/9910210.
36. E. Tzamariudaki, these proceedings.
37. P.D.B. Collins, *An Introduction to Regge Theory and High-Energy Physics*, Cambridge 1977.
38. J.D.Bjorken, hep-ph/0008048; J.Bartels, H.Kowalski, hep-ph/0010345.
39. UA8 Coll., *Phys.Lett.* **B211** (1988) 239; *Phys.Lett.* **B297** (1992) 417; *Phys.Lett.* **B421** (1998) 395.
40. ZEUS Coll., *Phys.Lett.* **B315** (1993) 481; H1 Coll., *Nucl.Phys.* **B429** (1994) 477.
41. J. Collins, *Phys.Rev.* **D57** (1998) 3051, erratum.
42. H1 Coll., *Z. Phys.* **C76** (1997) 613.
43. H1 Coll., contr. paper to ICHEP 1998, Vancouver.
44. H1 Coll., F.P. Schilling, proceedings DIS 2000, Liverpool.
45. ZEUS Coll., contr. paper to EPS99, Tampere.
46. H1 Coll., R. Stamen, proceedings DIS 2000, Liverpool; L. Favart, these proceedings.
47. A. Sznadjer, these proceedings.
48. CDF Coll., *Phys.Rev.Lett.* **84** (2000) 5043.
49. CDF Coll., *Phys.Rev.Lett.* **85** (2000) 4215.
50. F. Hautmann, D.E. Soper, *Phys.Rev.* **D63** (2000) 011501; V. Khoze, A. Martin, M. Ryskin, hep-ph/0007083; and references therein.